A&A manuscript no.
(will be inserted by hand later)
Your thesaurus codes are:
11.01.2, 11.10.1, 11,17.4 CTA102

Multiband VLB1 observations of CTA 102

F. T. Rantakyrö[1,2] *, L. B. Bååth[2], D. Dallacasa[4,5], D. L. Jones[6], and A .E. Wehrle[7]

[1] Dept. of Astronomy and Astrophysics, University of Gothenburg, S-412 96 Gothenburg, Sweden
[2] Onsala Space Observatory, S–439 92 Onsala, Sweden
[3] Centre for Imaging Technologies, Halmstad University, S-301 18 Halmstad, Sweden
[4] Istituto di RadioAstronomia – CNR, Via Gobetti 101, 1-40129, Bologna, Italy
[5] Dipartimento di Astronomia, via Zamboni 33, 1-40126 Bologna, Italy
[6] Jet Propulsion Laboratory, Pasadena CA 91109, USA
[7] Infrared Processing and Analysis Center, Jet Propulsion Laboratory, California Institute of Technology, Mail Code 100-22, Pasadena CA 91125,-USA

submitted; accepted date

Abstract. The source CTA102, known to exhibit low frequency variability, has been observed at six epochs (three at λ32 cm, two at λ18 cm, and one at λ1.3 cm) with intercontinental VLBI arrays. On the basis of the changes observed in the structure, we believe that the flux density variations at these wavelengths are due to intrinsic processes and not due to interstellar scintillation. This source exhibits behaviour suggestive of being expanding with a very high apparent transverse velocity.

Key words: galaxies: active – galaxies: jets - quasars: CTA102

1. Introduction

The quasar C'J'A102 (QSO 2230+114, $z = 1.037$) was the first radio source for which variations in the flux density were reported (Scholomitski 1965). The time scale of the variations led Sholomitski to deduce a linear size of 0.1 pc for the radio emitting region. An angular size of 10 milliarcseconds (mas) was deduced by Slish (1963) from the spectral turnover, but at the redshift distance of CTA102 this implies that the region responsible for the synchrotrons emission is larger than deduced from the variability time scale. With the inferred angular size the brightness temperature of the variable component would exceed the inverse Compton limit and a very large X-ray flux density should be observed. The dilemma of "Superluminal Flux Variations" (Romney et a}. 1984) can be solved by either an intrinsic model based on bulk relativistic motion of the radio emitting material (Blandford & Königl 1979; Scheuer & Readhead 1979), or an extrinsic model based on refractive interstellar scintillation (Rickett et al. 1984; Rickett 1986). There is strong evidence that in the well studied superluminal radio sources the observed changes in structure are intrinsic, but there is also strong evidence that the flux density variations seen in pulsars and some extragalactic sources (at wavelengths $\gtrsim 30$ cm) are due to scattering along the line of sight (Cawthorne & Rickett 1985; Gregorini et al. 1986; Spangler et al. 1989).

VLBI is the only technique capable of directly observing changes in the apparent morphology of CTA102 aud of deducing whether these changes are intrinsic or extrinsic. CTA 102 is a low frequency variable radio source, and thus is a candidate for either extrinsic or intrinsic variability models, or even a combination of the two models.

The arcsecond scale structure of the source is dominated by a central core and two other components (Antonucci & Ulvestad 1985; Spencer et al. 1989). At λ18 cm the stronger has a flux density of 0.2 Jy and is located at ~1.6 arcsec in P.A. -140° while the weaker is only 0.1 Jy at 1.0 arcsec in P.A. --40°. Both components have a steep spectrum.

Our observations were made at three different wavelengths: 32, 18, and, 1.3 cm. The observations at 18 and 1.3 cm used the standard VLBI setup, while the the λ32 cm used nonstandard VLBI receivers and feeds, these were in use for VLBI spectral line observations of redshifted HI in 0235+164. This is just below the frequency range where the amplitude of slow flux density variations begins to increase (Rickett et al. 1984).

2. Observations and data reduction

We have observed CTA 102 with a global VLBI array at six epochs: on August 12, 1983 (epoch 1983.61), Au-

Send *offprint requests to*: F. T. Rantakyrö
* Present *address*: Istituto di Radioastronomia - CNR, Via Gobetti 101, 40129 Bologna, Italy.

gust 12, 1984 (epoch 1984.61), December 15, 1984 (epoch 1984.96), May 29, 1988 (epoch 1988.41), June 13, 1989 (epoch 1989.45), and June 141992 (epoch 1992.45), in all cases using left circular polarization (IEEE standard). The wavelengths and telescopes used are listed for each epoch in table 1 (λ32 cm), table 2 and table 3 (λ18 cm), and table 3 (λ1.3 cm), The data were recorded with a MkII recording system at a bandwidth of 1.8 MHz.

2.1. *Observations at λ32 cm*

The data were processed on the VLBI processors at NRAO, Charlottesville and California Institute of Technology. The uv-coverage was sufficient to map the general structure of the source, but artifacts on very large scales may remain due to the limited coverage of the very short baselines. This may be the cause of the northern feature at ~20 mas from the core, in figure 1. Attempts were made to remove the northern feature by applying a 'window' in the CLEAN-self-calibration procedure, but we were unable to remove this feature.

Table 1. Telescopes used at λ32 cm

Epoch	ARE[1]	KIR[2]	JB[3]	OVRO	NRAO
	US	SWE	UK	US	US
1983.61	*X*	*x*	-	*x*	*x*
1984.61	x		x	x	x
1984.96	**X**	**x**	**x**	**x**	**x**

[1]Arecibo [2]Kiruna [3] Mark II

'J'able 2. European and South African telescopes used at λ18 cm.

Epoch	Bologna	Bonn	Crimea	Hartebeesthoek
	IT	FRG	USSR	SA
1988.41	x	**x**	**x**	**x**
1989.45	**x**			

Epoch	Jodrell Bank	Onsala	Torun	Westerbork
	UK	SWE	PL	NL
1988.41	**x**	**x**		**x**
1989.45	**x**	**x**	x	**x**

.?,2. *Observations at λ18 cm*

All data were correlated at the JPL/Caltech Block II correlator at Caltech, USA. With the large number of participating antennas we obtained a very good uv-coverage.

Table 3. American telescopes used at λ18 cm.

Epoch	Arecibo	Fort Davis	Haystack	Iowa
1988.41	**x**	**x**	**x**	**x**
1989.45	-	**x**	**x**	**x**

Epoch	Kitt	NRAO	OVRO	Pietown	VLAE8
1988.41	-	**x**	**x**	**x**	**x**
1989.45	*X*	*x*	*x*	*x*	*x*

2,3. Observations *at λ1.3 cm*

The data were correlated at the JPL/Caltech Block II correlator at Caltech, USA. The observation was scheduled as an ad-hoc EVN observation including Crimea. Due to problems with the Crimea antenna, there were only 4 antennas operational. The uv-coverage was adequate only to map the small scale structure in the source.

!I'able 4. Telescopes used at λ1.3 cm

Epoch	Onsala	Bonn	Metsähovi	Bologna
	SWE	FRG	FIN	IT
1992.45	'x	**x**	**x**	**x**

2.4. Reduction of data and *calibration*

All data processing was done within AIPS (Fomalont 1986). At each telescope, the amplitudes were calibrated using measured system temperatures and a previously measured gain curve (Cohen et al. 1975). The self calibration technique (Schwab & Cotton 1983) was used to correct for phase fluctuations at each antenna. The amplitude calibration was corrected in the last stage of the self-calibration- process by comparing the amplitudes on baselines of comparable lengths and position angles. We estimate that the resulting flux density scale in the images is correct to within 5% at λ18 cm, and within 10% at λ32 cm and λ1.3 cm.

2.5. Quality *of images*

As a measure of the quality of the images, we have used the measured peak level compared to the noise rms measured in an extended region far from the source. table 5 summaries the result of these measurements. The SNR is similar for the first three epochs, but is higher for the fourth and fifth epochs. The SNR in the first three images is limited by the poorer uv-coverage arrd shorter observation time. Due to the smaller number of antennas in

the 1992.45 epoch and a lower flux density, we measure a relatively low SNR.

Table 5. Parameters for the quality of the images. Signal to noise ratio is given in dB's

Epoch	λ [cm]	Peak Flux [Jy]	RMS [mJy]	SNR [dB]
j 983.61	32	2.28	4.8	27
1984.61	32	1.98	5,5	26
1984.96	32	2.04	7.3	24
1988.41	18	2.14	0.6	35
1989.45	18	3.8	2.5	32
1992.45	1.3	1.1	4.9	24

2.6. *Position measurement errors*

These *errors* are errors obtained from the LSQ fit to the visibility data. The error given in this article will be three times the errors from the fits which are, in general only valid for the model for which they are calculated. Any flux scale error is not included into the error estimates.

3. Results

The position of the phase center in self-calibrated VLBI images is arbitrary. The core at each epoch has been chosen to be the bright northern component in the elongated central feature. Hereafter, all future references to coordinate positions will be in relation to the position of the core. To help with translating from the core based coordinate system to the coordinates given *in* the images, we give the positions of the core to the phase center of the image for all epochs made at λ32 cm and λ1.3 crn (table 6). The labeling of the components were chosen as shown in tables 7- 9.

3.1. Structure in λ = 92 cm images

The images from the first three epochs at λ32 are presented in figure 1 where, for comparison, the contour levels and the restoring beams are the same for all three epochs. Three major components are visible in the images: a bright double knot structure containing the core and a jet component, and a small feature north of the central knot. Parameters for these components were obtained by fitting Gaussian source models to the image (see table 7). **The best fit was achieved by fitting two Gaussian components to the central double knot and one component to the northern knot at all three λ32 cm** epochs. The core, D, is assumed to be the bright northwestern component in the central double-knot at each epoch. The positions of the fitted Gaussian components are measured relative to the core, D, at each epoch,

Table 6. Distance [mas] of the core, D, at each epoch, to the phase center of the image at each epoch.

	Epoch			
	1983.61	1984.61	1984.96	1992.45
$\Delta\alpha$	-0.0540.1	-0.240.2	-01140.1	-0.01±0.02
$\Delta\delta$	0.130.1	0.540.2	0.240.1	0.06±0.02

3.2. *Structure* in λ = *18 cm images*

Contour images from the first and second λ18cm epochs ate presented in figure 2. With no Hartebeesthoek telescope *in* the second λ18 *crn* epoch the actual resolution is 22x3 mas in a position angle of – 13°. Both images use the same surface brightness contour-levels to take advantage of the higher dynamic range. 'I'he fuUy cleaned field is substantially larger than that shown, but contains no significant features. Two major components are visible: a bright component elongated in the NS direction, and an extended weaker knot SE of the brightest component.

We fitted three Gaussian components to the uv-data (Lerner 1995), although in genera] a four component fit yielded a better fit to the data. The parameters of the Gaussian fits are listed in table 8. Due to the large difference in time and wavelength from the λ32 cm epochs, we have elected to label the components in the jet as E0, and El. We will discuss the identification of these with the λ32 cm epochs, later. The result of this identification has been inserted into the table where a positive identification was possible. A question mark indicates a tentative identification.

3.3. *Structure in λ = 1.3 cm* images

The image from the 14 June 19920992.45 epoch) is shown in figure 3. The shown area is smaller than in figure 2. We have plotted one level deeper in this image than in figure 1. At this epoch there is a strong central component with a short bright extension in a position angle coincident with that of the jet seen at λ 18cm and at λ 32cm. There is also a faint component at a PA of 130°. The distance and PA of these components correspond to the two northern central components seen at the two λ 6 cm at epochs 1987.45 and 1988.45 (Wehrle & Cohen 1989). This suggests that the northern component at λ18 cm is the core, due to the flatter spectrum of this component. The extended jet at PA≈130° at a distance of 12 mas is not visible at this wavelength, indicating a steep spectral slope for these features, expected from the synchrotrons radiation from a shock in the jet. We have designated the core component, D, as in the previous observations, and **due to the large time and wavelength difference we have elected to label the SE components as F1 and F2,** where F2 is the component closest to the core. The identification of these with the earlier epochs will be discussed in

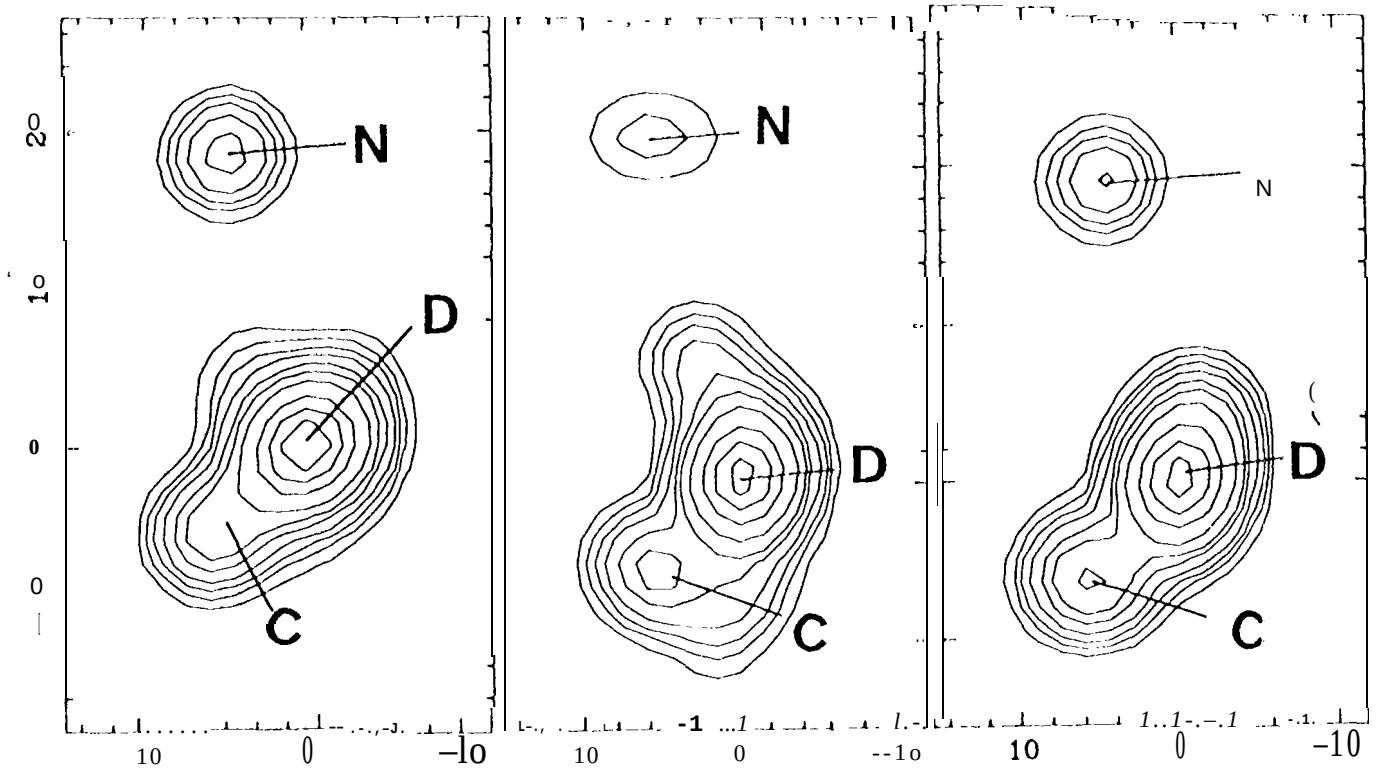

Fig. 1. λ32 cm images. From left to right: a 12 August 1983. b 12 August 1984. c 15 December 1984. Peak contour flux = 2.3 Jy/Beam. Contour intervals are chosen as (-3.o, 3.0, 5.0, 7.0, 10.0, 15.0, 20.0, 30.0, 50.0, 70.0, 90.0)x20 mJy/beam. The restoring beam was a 5mas (FWHM) circular Gaussian in all three images, The coordinates axes are in mas and refer to the phase center of the images

Table 7. Parameters of the Gaussian components fitted to the λ32 cm images. Arr and Δδ are the angular distances from the core at respective epoch. The distance of the cores from the phase center of the images at each epoch are *given in* **table 6. The errors cited in this table represent three times the standard errors from the fit of the Gaussian components to the images. S_{int} is the integrated flux density of the component. Any flux scale error is not included**

-Epoch	ID32	A [mas]	α	Δδ [mas]	major axis [mas]	minor axis [mas]	position angle [Deg]	peak flux [Jy]	S_{int} [Jy]
1983.61	N	4.9±0.1		18.44-0.1	1.830.2	–).140.2'	118±12	0.37±0.01	0,4040.01
1983.61	D				3.9±0.2	2.1±0.2	138±6	2.2±0.1	3.040.2
1983.61	C	5.7±0.2		-5.54-0.2	2.040,9	1.330.9	107460	0.6±0.1	0.6±0.1
1984.61	N	5.6±0.3		21.6±0.2	6.240.6	2.7±1.2	87±12	0.12±0.01	0.2240.03
1984.61	D	·			4.14.0.3	1.7±0.3	178±6	2.040.1	2.7±0.2
1984.61	C	4.940.6		-6,610.5	≤7.7	≤7.7		0.4±0.1	0.840.2
1984.96	N	4.8±0.2		18.830.2	1.640.3	1.440.3	109±60	0.3230.01	0.3540.03
1984.96	D				4.730.2	1.1±0.6	164±6	2.030.1	2.840.2
1984.96	C	6.040.2		-6.540.2	≤2.7	≤2.7		0.650.1	0.7±0.1

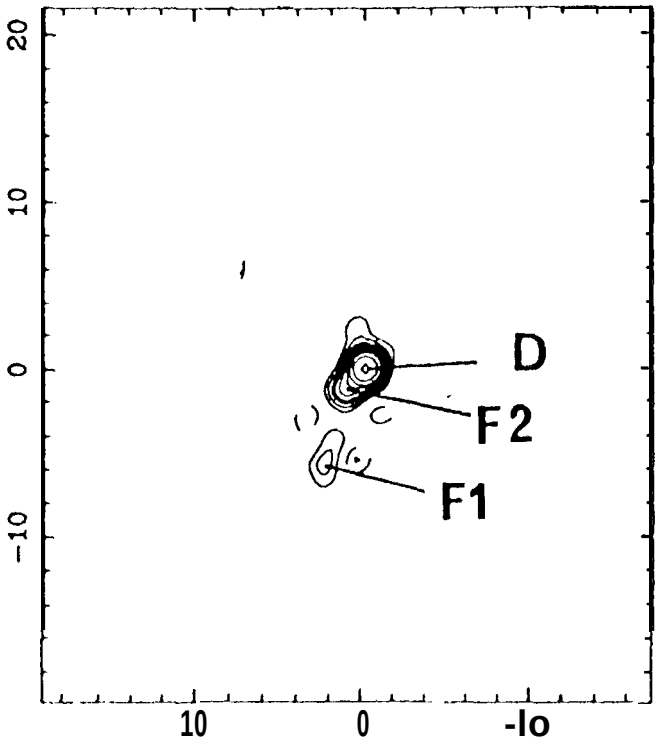

Fig. 3. **Map from 14 June 1992** at λ1.3cm. **Peak contour flux** =1.1Jy/Beam. **Contour intervals arc chosen as (-3.0, -1.5, 1.5, 3.0, 5.0, 7.0, 10.0, 15.0, 20.0, 30.0, 50.0, 70.0, 90.0)x20 mJy/beam. The restoring beam was a 1.5 mas (FWHM)** circular Gaussian. The coordinates axes are in mas and refer to the phase center of the image

cause a shift of the core on the sky of ~2 mas between our observing wavelengths ($\lambda 32\,cm - \lambda 1.3\,cm$). Thus care will be taken so that proper motion measurements will not involve data from different wavelengths in the same LSQ-fit.

To facilitate the identification of components at all three wavelengths, we have plotted the position of the components relative to the core, D, at each epoch, including the two epochs try Wehrle & **Cohen** (1989), in figure 4. The errors and positions from the two epochs by Wehrle & Cohen (1989) are all direct measurements and estimates from the published images. From the position of the components we suggest that F1 is component E1 seen in the two λ18 **cm** epochs. Component E0 might be component **C at a later epoch, but the large difference in observing epoch and wavelength makes this identification uncertain.** 'l'here is no other clear identification of components between the three wavelengths. The actual identification between different wavelengths are not used when measuring the proper motion, as the proper motion measurements are done independently at each frequency.

Table 9. Parameters of the Gaussian point-source components fitted to the 1.3cm image, 1992.45 epoch. Aa **and A6 are the angular distances from the core. The distance of the** *cores* **from the** phase center **of the images at each epoch are given in table 6. The errors cited in** this table represent three times the standard errors, in this fit. **Any flux scale error is not included. We** have chosen **to label the components as F1, F2,** and D, to **avoid confusion with components at other wavelengths.** S_{int} **is the integrated flux density of the** component. The λ18 **cm** counterpart have **been inserted where an identification was possible**

$ID_{1.3}$	ID_{18}	$\Delta\alpha$ [mas]	$\Delta\delta$ [mas]	S_{int} [J y]
D	D	-		I.1O*O.O2
F2	-	1.1640.07	-1.26±0.07	0.25±0.02
F1	E1	2.5640.29	-5.66±0.45	0.09±0.03

4. Discussion

In the following discussion, it is assumed that the observed redshift, z = 1.037, is cosmological in origin with H_0 = 100 h kms^{-1}Mpc^{-1}, and q_0 = 0.5. Using these parameters, 1 mas then corresponds to a distance of 4.2 h^{-1} pc. At the measured redshift, an angular velocity of 1 mas yr^{-1} then corresponds to an apparent transverse velocity of u = 28 h^{-1} c.

In the following, we discuss the proper motion of components, importance of extrinsic (refractive) scintillation and intrinsic structural changes, and the curvature of the jet in CTA102.

4.1. Proper motion of the components

The proper motion of the components relative to the core (see table 10) was obtained from the measured positions of the Gaussian components (see tables 7 – 9) at several epochs and observations by others (Bååth 1987; Wehrle & Cohen 1989). To avoid problems with spectral index effects, resolution problems, and the previously discussed **problem of determining the location** of the *core* between different wavelengths (see section 3.4), we make a separate least squares fit for each component for all positions at each frequency. Due to the poorer resolution along the δ-axis (22 mas HPBM compared to 3 mas HPBM), we only measure the proper motion along the α-axis for the 1988.41 and 1989.45 epochs.

A plot. of distance from the core as a function of time, for all components showing a significant proper motion is shown in figure 5. Each line represents a least squares fit to the data at each wavelength. The LSQ fit to the component E1, suggests that the component is stationary or is moving with a low apparent velocity. Although the shift in location of the core is wavelength dependent (see section 3.4) the rate of change in the position of components with respect to the core (for each wavelength),

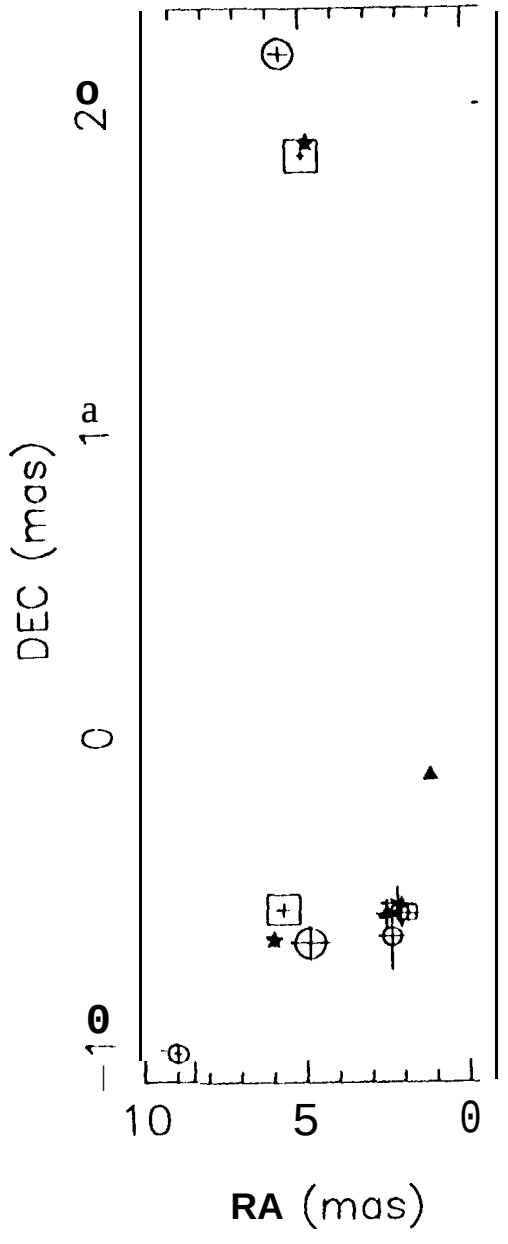

Fig. 4. The position of the fitted Gaussian components arc **plotted relative to the** core, *D*. **The symbols represent the following epochs: Large** □ **-1983.61, 0-1984.61, * -1984.96, * - 1987.45, small** □ **- 1988.41, 0- 1988.45, 0- 1989.45, and filled A -1992.45**

should not be affected by this phenomenon. Both LSQ fits to λ32 and λ18 are in support of a large proper motion for the component at the end of the jet, labelled E0 and C. If the expansion is along the PA∼135° as suggested by the large scale structure the measured proper motion along the α-axis then corresponds to $\mu \approx 0.8 \pm 0.3$. Such a large proper motion is unprecedented and should be regarded with caution. The errors are quite large, due to the poor north-south resolution and more epochs are needed to investigate this. Wehrle and Cohen (1989) have

Table 10. Apparent velocities. r_0 is the distance from the core. μ and β arc obtained from a least-squares-fit to all measured positions of a component at a given wavelength. The errors are three times the standard error from the fit to the components

ID	Epoch	λ [cm]	r_0 b ']	μ_{app} [mas/yr]	β_{app} [v/c]
N	1983.61	32	19.0±0.3		
	1984.61	32	22.33.0.5		
	1984.96	32	19.440.3	0±0.6	0±17
E1	1987.45°	6	5.940.5		
	1988.45°	6	6.240.5	0.3±0.6	8±17
E1	1988.41[b]	1 8	1.940.1		
	1989.45[b]	1 8	2.4±0.4	0.5± 0.4	14±11
c	1983.61	32	7.9±0.3		
	1984.61	32	8.2±0.8		
	1984.96	32	8.840.3	0.640.2	17±6
E0	1988.41[b]	1 8	8.530.2		
	1989.45[b]	1 8	9.040.1	0.540.2	14±6

" *From* observations by Wehrle & Cohen (1989)
[b] Limited to proper motion along a-axis

shown that at λ6 cm an upper limit to motion of components along the principal axis of the structure (excluding the tail (E0)) in the source is, $\mu \lesssim 0.5$ mas/year. In an extreme case where motion is along PA∼168°, arr upper limit is $\mu \lesssim 1.0$ mas/year.

The slopes at λ32 cm, and λ18 cm, and the upper limit at λ6 crn arc all consistent with a proper motion, $\mu = 0.6 \pm 0.2$, at the outer end of the jet. There appears to be an increase in the transverse velocity of a component as a function of distance from the core (see table 10). Such a scenario would also fit the λ6 crn measurement of a lower velocity closer to the core (Wehrle & Cohen 1989). Unless one wants to introduce an acceleration of the shock/plasma flow this suggests a change in the apparent viewing angle. An increase in the apparent transverse velocity could be caused by either an increase or decrease in the angle to our line of sight, depending on the starting point. By combining this with observations of the intensity of the jet as a function of distance from the core, we can determine whether the angle is decreasing or increasing. This will be discussed later.

To obtain a measure of the minimum γ we use the following approach. By maximizing the effect of the viewing angle, and assuming $\beta_{app} >> 1$, a minimum, γ_{min}, can be calculated:

$$\gamma_{min} = \sqrt{1 + \beta_{app}^2} \quad (1)$$

Using the measured β_{app} from table 10, the largest γ_{min} is 17. This value of γ is high but not unreasonably high. Recent models of jet formation and acceleration allow velocities of the underlying plasma flow of up to $\gamma \sim 40$ (Rees 1994). Also important is that we observe the appar-

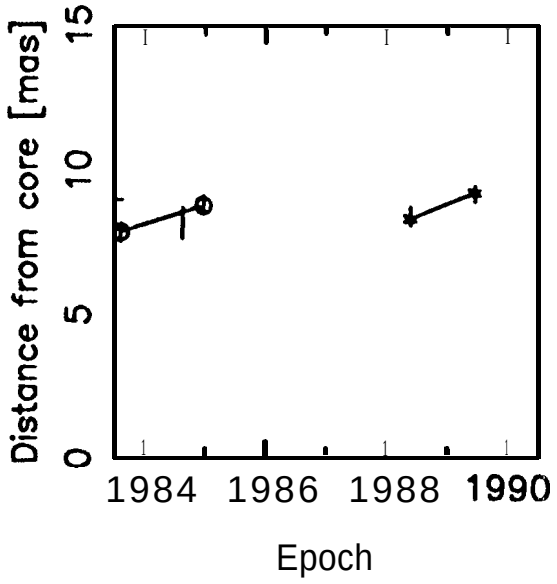

Fig. 5. The distance from the core as function of time for components C - ○, E0 - *. The errors are three times the standard error from the fit to the components. The lines are the result of a LSQ fit to the position of a component at each wavelength

ent pattern speed, which need not be that of the plasma in the jet.

The motion of the components doesn't seem to follow a straight or a simply curved path. To investigate this further more data are needed.

4.2. Extrinsic scattering or intrinsic variations

Continuum observations of CTA102 with polarization position angle, percent polarization and total flux density are plotted in figure 6. CTA102 is part of a sample selected for strong low frequency variability. The question is whether these variations are more likely to be intrinsic or extrinsic. Although the extrinsic (refractive scintillation) model is likely to apply to many low frequency variables, we believe that an intrinsic model is more applicable to CTA 102. The six main reasons for believing this are:

1. CI'A102 is at a high galactic latitude (b= −38.60), thus giving a relatively small path-length through the galactic disc where most of the scattering matter is located (Rickett 1986).
2. Low frequency variations in this source have been observed at frequencies <1 GHz (Dennison et al. 1984; Spangler et al. 1989; Mantovani et al. 1990). Assuming that the low frequency variations are due to refractive scattering in the interstellar medium located in the galactic disc, the following relations can be derived for a gaussian brightness distribution (Rickett 1986):

$$\tau = L\frac{\csc|b|\sqrt{\theta_s^2+\theta_I^2}}{1.7v} \quad (2)$$

$$\theta_s = \theta_0\sqrt{\csc|b|}\lambda^2 \quad (3)$$

$$m = 0.5\frac{\theta_s}{\sqrt{\theta_s^2+\theta_I^2}} \quad (4)$$

where τ is the extrinsic variability timescale in days, L the thickness of the scattering medium in the galactic disc in parsec, O, is the scattering angular size in mas, 6 ', is the intrinsic angular size of the object in mas, θ_0 is a parameter dependent of the scattering medium characteristics in mas, v is the velocity in km/s of the scattering irregularities in the galactic disc, *b is* the galactic latitude in degrees, λ is the observation wavelength in m, and m is the fractional rms variability of the radio flux. In our case b = -38.6°, θ_0 arrd θ_I are constants, θ_0 -8 mas (Fanti et al. 1987), and assuming a component size $\theta_I \sim 5$ mas, by combining equations 3 and 4 we obtain:

$$m = \sqrt{\frac{0.25}{1-1\left(\frac{\theta_I}{\theta_0}\right)^2\lambda^{-4}\sin|b|}} \quad (5)$$

The fractional variability at λ32 is then only 6% compared to 28% at λ73 cm[1], suggesting that even if the refractive scattering in the interstellar medium is an important factor at decimetric wavelengths it should not be dominant at our observing wavelengths.

3. The total flux density has been nearly constant over a 10 year time period with the exception of a few outbursts (figure 6), seen at all three wavelengths. These are all seen first at short wavelengths and later at longer wavelengths with a lower amplitude. This behavior is typical of synchrotrons radiation from a shock propagating down a plasma flow (Marscher et al. 1992). Furthermore outbursts are coincident with rapid changes in polarization angle and degree of polarization (see figure 6), suggesting the birth of a new component and not a scattering event.
4. Observations of CTA102 with the EGRET telescope at the hig}l-energy γ-ray waveband have shown that the source exhibits a strong γ-ray luminosity, L_γ = 5 x 10^{47} ergs s- [1] (Nolan et al. 1993). This luminosity dominates the emission seen at al} other wavebands, a common feature among BL AZARs. The common explanation for the high L, is that the emission is the result of a beamed jet with a high Lorentz factor (Blandford & Königl 1970).
5. The observed rapid superluminal expansion has followed the same general position angle, and the expansion can be seen at large distances from the core (figure 4; table 10). There is also an observed increase of the apparent superluminal motion with dis-

[1] This wavelength was chosen since it represents the wavelength where strong scintillations has been seen

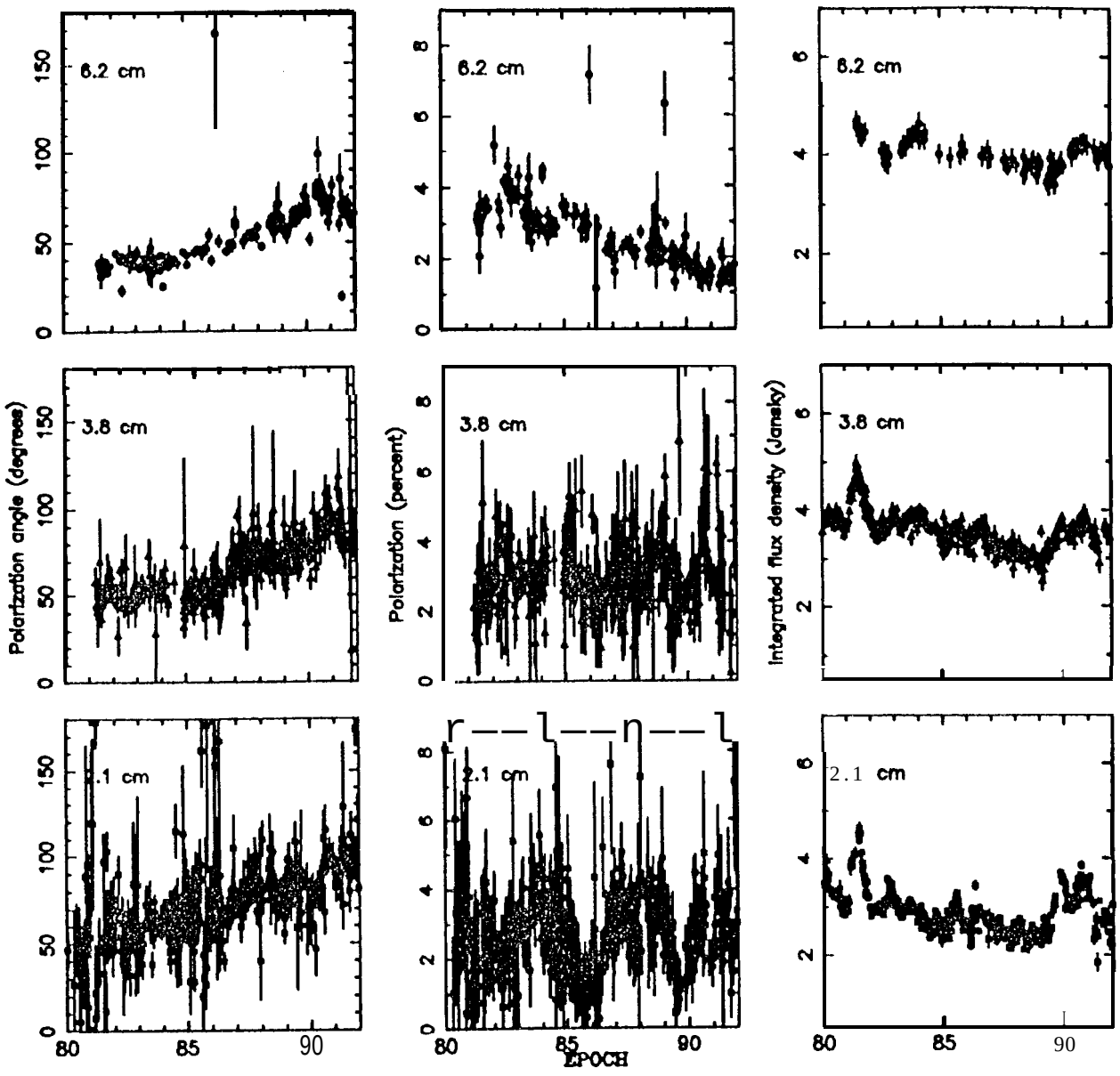

Fig. 6. Plots of polarization angle, fractional polarization, and the total flux density of the source CTA102, at wavelengths λ6.2 cm, λ3.8 cm, and λ2.1 Cm from 1980 to 1991. Courtesy of H.D. Aller & M.F. Aller, University of Michigan. The data are the unaveraged and uncorrected observations. See Aller et al. (1985) for the period 1974.6 -84.9

tance from the core that we attribute to a change in the viewing angle, θ. The position angle, PA, of the jet at mas scale coincides with that of the large scale structure observed with MERLIN and VLA (Spencer et al. 1989; Antonucci & Ulvestad 1985).

6. The apparent intensity of a component seems to decrease with distance from the core or with time. Assuming that the radiation is from synchrotrons radiation, such a decrease can be due to both cooling by internal radiation processes and to a change in the viewing angle, θ. The change of the observed intensity of a relativistically moving source can be written as (Bland ford & Königl 1979):

$$I_{app} \propto \frac{I_{com}\delta^a}{\sin\theta} \quad (6)$$

where I_{com} is the comoving intensity, a is a model dependent parameter (typically a - 2 -- 4), and the doppler factor, δ, is defined as:

$$\delta \quad \frac{1}{\gamma(1 - \beta\cos\theta)} \quad (7)$$

Hence a small change in the viewing angle can cause a very large change in the Doppler boosting, thus explaining the decrease of the apparent intensity of the components.

One difficulty of assuming that the superluminal motion and the variability in CTA102 is caused by intrinsic effects is that it has the largest proper motion known in any extragalactic radio source. This makes CTA 102 a unique object, conspicuous on plots of proper motion vs. redshift (Cohen 1987). However, this argument cannot be a very strong objection. CTA102 could very well be at the extreme end of a distribution of γ's, particularly since it is only one of the few extragalactic sources detected by the Compton GRO (Fichtel et al. 1994).

4.3. *The Northern Feature*

As to date there is no clear evidence of a counter-jet seen in a superluminal source. *In* the standard unified model the one- sided structure seen in superluminal sources is attributed to the beaming effect dominant in relativistic plasma jets (Blandford & Königl 1979). CTA 102 exhibits many features typical of a beamed jet, high variability, superluminal motion, small size, and a high intensity. Therefore we do not expect the source to show any counter-jet. The north component seen at λ 32 cm, NO, is suggestive of a counter-jet, and the images at λ 6 cm by Wehrle & Cohen (1989), also show at one epoch a low intensity feature at a similar position. This component is, however, not confirmed at our observations at λ18 cm, indicating that it is either resolved at that wavelength, has a steep spectral index, is time dependent, or is an artifact of our instrument at λ32 cm.

5. Conclusions

We have presented three λ32 cm, two λ18 cm, and one λ1.3 cm image of the source CTA102. With VLBI data taken at three different λ and at different epochs and applying special techniques we were able to follow structural changes in the source. Additional information can be inferred using published (Aller & Aller 1985) and unpublished (Courtesy of Aller & Aller for the data from 1983 to date) flux density monitoring data. Combining all this information we can draw the following tentative conclusions:

We have shown that the variability is connected with changes in the degree of polarization and polarization angle, as expected of synchrotrons radiation from a shock. The delay between outbursts at different wavelengths is consistent with the propagating shock model (Marscher et al. 1992). We have also shown that the expansion seems to follow a similar position angle, and that expansion can be seen at all wavelengths. Therefore, although refractive scintillation may play an important part at frequencies $\ll$1GHz, it does not make a significant contribution to the variability seen in our observations, which we think is due to intrinsic causes.

- By doing a LSQ fit to the measured positions of fitted Gaussian components for each component at each wavelength, including two images by other authors, and fitting Gaussians to the uv-data, we show that the data suggests that there appear to be large superluminal motions in the source, the motion doesn't follow any straight lines or ballistic paths and further data arc needed to investigate this phenomena further. The observations also seem to suggest that the apparent motion appears to increase with distance from the core. Going from v $\approx$0 c close to the core and increasing to v approx 15$\pm$6 at distances$\gtrsim$10 mas from the core. We suggest this to be an effect of a change in viewing angle.
- We also see at the two λ 18 crn epochs a *decrease* in surface brightness with distance from the core. The beaming hypothesis combined with the increase in apparent velocity, then suggests that the jet is pointing almost directly towards us close to the core and is bending *away* from the line of sight as the distance to the core increases. We hope to confirm this result with new observations.

The data is sparse in both time and frequency space, thus more observations are needed to investigate the existence of superluminal motion in this source.

Acknowledgements. We would like to thank H.D. Aller & M.F. Aller for the courtesy of allowing us to use the flux monitoring data of CTA102 previous to publication, Prof. R.S. Booth for help in proofreading the manuscript, and M.S. Lerner for the use of his software. Fredrik T. Rantakyrö **acknowledges support for his research by the European Union under** *contract* **ER13CHGECT920011. Onsala Space Observatory at Chalmers University of Technology is the Swedish National Facility for Radio Astronomy. Part of this research was carried out at the Jet Propulsion Laboratory, California Institute of Technology, under contract with the National Aeronautics and Space Administration.**

References

Aller, H. D., Aller, M.F., Latimer, G. E., Hedge, P.E. 1985, ApJS, 59, 4, 513

Blandford, R.D., Königl, A. 1979, ApJ, 232, 34

Bååth, L.B. 1987, in: Superluminal Radio Sources, eds. Zensus, J. A., Pearson, T.J. Cambridge University Press, p206

Cawthorne, T. V., Rickett, B.J. 1985, Nature, 315, 40

Cohen, M.H., Moffet, A. T., Romney, J. D., et al. 1975, ApJ, 201, 249

Cohen, M. H. 1987, in: Superluminal Radio Sources, eds. Zensus, J. A., Pearson, T. J., Cambridge University Press, 306

Dennis. on, B., Broderick, J. J., O'Dell, S.T., et al. 1984, APJ, 281, 1,55

Fanti, R., Gregorini, L., Padrielli, L., Spangler, S., 1987, in Superluminal Radio Sources, eds Zensus, J. A., Pearson, T. J., Cambridge University Press, 202

Fichtel, C. E., Bertsch, D. L., Chiang, J., et al. 1994, ApJS, 94, 551
Fomalont, E.B. 1986, in: Synthesis Imaging, eels. Perley, R. A., Schwab, F. R., Bridle, A.H., NRAO, 215
Gregorini, L., Ficarra, A., Padrielli, L. 1986, A&A, 168, 25
Lerner, M, S., 1995, in: Millimeter VLBI Observations - Hybrid Mapping and Model fitting, Licentiate Thesis, in preparation
Mantovani, F., Fanti, R., Gregorini, L., Padrielli, L., Spangler, S. 1990, A&A, 233, 535
Marcaide, J. M., Shapiro, 1.1., Corey, B. E., et al. 1985, A&A, 142, 71
Marscher, A. P., Gear, W. K., Travis., 1992, in: Variability of Blazars, eds Valtaoja, E., and Valtonen, M., Cambridge University Press, 85
Nolan, 1'.1.., Bertsch, D. L., Fichtel, C. E., et al. 1993, ApJ, 414, 82
Rees, M. J., 1994, in : *Multi-Wavelength* Continuum *of AGN*, IAU Symposium No 159, eds Courvoisier, T. J-L., Blecha, A., Kluwer Academic Publishers, 239
Rickett, B. J., Colts, W. A., Bourgois, G. 1984, A&A,]34, 39o
Rickett, B.J. 1986, ApJ, 307, 564
Romney, J., Padrielli, L., Bartel, N., et al. 1984, A&A, 135, 289
Rudnick, 1,., 1982, in *Extragalactic* Radio Sources, IAU Symp. 97, eds Heeschen, 1). S., Wade, C. M., D. Reidel Publishing Company, 47
Scheuer, P.A.G., Readhead, A.C.S. 1979, Nature, 277, 182
Scholomitski, G.B. 1965, SOVAJ, 9, 3, 516
Schwab, F., Cotton, W. 1983, AJ, 88, 688
Slish, V.I. 1963, Nature, 199, 682
Spangler, S., Fanti, R., Gregorini, L., Padrielli, L. 1989, A&A, 209, 315
Spencer, R. E., McDowell, J. C., Charlesworth, M., et al., 1989, MNRAS, 240, 657
Wehrle A. E., Cohen, M., 1989, ApJ, 346, 1,69

This article was processed by the author using Springer-Verlag LaTeX A&A style file *L-AA* version 3.